Appl. Phys. B 61, 421–427 (1995)

Applied Physics B Lasers and Optics

Polarization-spectroscopic measurement and spectral simulation of OH ($A^2\Sigma$–$X^2\Pi$) and NH ($A^3\Pi$–$X^3\Sigma$) transitions in atmospheric pressure flames

A.A. Suvernev, A. Dreizler, T. Dreier, J. Wolfrum

Physikalisch Chemisches Institut, Universität Heidelberg, Im Neuenheimer Feld 253, D-69120 Heidelberg, Germany
(Fax: + 49-6221/56-4255)

Received: 2 May 1995/Accepted: 12 June 1995

Abstract. Polarization spectroscopy has been used to investigate the electronic bands of OH ($A^2\Sigma$–$X^2\Pi$) and NH ($A^3\Pi$–$X^3\Sigma$) radicals generated in atmospheric pressure flames. The pump-beam intensity dependence of the polarization-spectroscopy signals of isolated lines in the R branches has been studied. It was found that significant saturation is noticeable for pump-beam intensities as low as 0.1 MW/cm^2. A detailed theoretical description inluding laser-bandwidth convolutions has been developed to model unsaturated polarization spectra of OH and NH. For OH, temperature evaluations have been performed in methane/air flames from fits to experimental R_1 band head spectral structures. The results are critically dependent on the degree of saturation in experimental spectra, instrumental bandwidth and the assumed coupling cases in the calculation of line-strength parameters. It is shown that saturation leads to an error of more than 60% in the temperature evaluation when a pump-beam intensity of 1 MW/cm^2 is used.

PACS: 33.00; 42.65

With the first implementation of Polarization Spectroscopy (PS) by Wieman and Hänsch [1] in their investigation of atomic hydrogen, molecular sodium and nitrogen dioxide, it became evident that this technique constitutes a main break-through in the advancement of high-resolution gas-phase saturation spectroscopy. The main advantage in polarization spectroscopy over conventional saturation spectroscopy is that no longer a decrease of absorption of a probe beam, caused by the simultaneous depletion of ground-state population due to a strong pump wave is detected, but rather the change of the complex refractive index of the medium induced by a polarized pump wave can be monitored on a controllable, almost zero background. This high-sensitivity quantum-state-specific technique ensures a coherent signal beam for remote sensing and enables high spectral resolution to be attained through velocity selectivity of crossed-beam arrangements. These features have made polarization spectroscopy a widely employed technique, e.g., for the detailed study of atomic transitions perturbed by electric fields [2], and for the unravelling of complex molecular spectra [3].

The principles of polarization spectroscopy are outlined in early publications [4, 5] and textbooks [6]. Therefore, for a general understanding of the method only the basic ideas are given here. In its most simple arrangement, a weak polarized probe beam and a stronger circularly or linearly polarized pump beam are crossed in a nonlinear medium under a small angle – either counter- or co-propagating. Depending on its crossing angle with respect to the unperturbed polarization direction, part of the probe-beam light can be monitored through a polarizer in front of a detector. When the laser frequency is tuned through a molecular transition, pump-beam radiation can be absorbed within degenerate (magnetic) Zeeman sublevels determined by the polarization state of the radiation field and the selected allowed electric-dipole transitions (P, Q, R branches). Due to m-degeneracy between the lower and upper states of the laser-coupled transition, the saturating pump beam produces unequal populations among the sublevels of the upper and lower states, which leads to an anisotropic distribution in the orientation of the dipole-moment vector. This, in turn, induces a birefringence in the sample. As outlined in [4, 6], rotation of the probe-beam polarization direction is caused by the differential absorption and refraction in the anisotropic sample of left- and right-circularly polarized components of the linearly polarized probe light. The probe beam interacts with those molecules that are located within the same velocity group selected by the pump- and probe-beam wave vectors. Therefore, Doppler-broadened or "zero-velocity" line shapes can be obtained, depending on whether pump and probe beams are co- or counter-propagating in the sample, respectively.

The capabilities of polarization spectroscopy have been recognized, especially as a means for improvement of the signal-to-noise ratio as compared to crossed-beam saturation spectroscopy [7]. Tong and Yeung [8] and

Zizak et al. [9] were among the first to apply polarization techniques to trace species detection in flames seeded with sodium. Later, Nyholm et al. [10] demonstrated the method for the detection of flame-generated species such as OH. The potentials of polarization spectroscopy for two-dimensional imaging of these species and single-shot temperature measurements were shown by Nyholm et al. [11, 12]. In both cases, for quantitative interpretation of results, the degree of saturation of the probed transitions are of decisive importance, since relative line-intensity ratios are easily perturbed in one-photon resonant transitions, even with low-intensity beams. In their work, these authors use the intensity ratio of only two transitions for the evaluation of the temperature. This method can lead to large errors if saturation effects are not considered. In a later study, Nyholm [13] demonstrated temperature measurements from Boltzmann plots of relative OH signal strengths, but without taking into account convolution effects from finite laser bandwidths in experimental spectra. These can be modeled properly only by spectral simulation. Polarization spectroscopy seems to be ideally suited for flame studies since in many circumstances optical access through birefringent windows is not necessary, eliminating the most severe background noise source-term.

In the present study, polarization spectra of OH and NH in atmospheric-pressure flames were investigated using vibrationless transitions in their $A^2\Sigma$–$X^2\Pi$ and $A^3\Pi$–$X^3\Sigma$ electronic band, respectively. Different spectral branches were recorded with co- and counter-propagating pump and probe beams of varying intensities, and the saturation behavior of individual transitions for specified beam geometries was studied. In addition, for both molecules, a spectral synthesis was performed showing the crucial role of line interference, laser-bandwidth effects and line-strength modeling for thermometry in flames.

1 Theory

In polarization spectroscopy, the anisotropy of the medium created by the pump beam is due to selective absorption within the degenerate magnetic sublevels of quantum states coupled by the laser radiation. Consequently, the linearly polarized probe beam experiences different absorption and dispersion for its right- and left-circularly polarized components. The difference in absorption leads to a rotation of the plane of polarization, whereas the difference in indices of refraction results in a small amount of ellipticity in the probe-beam polarization. In the limit of no saturation, the signal intensity was derived in [4].

An expression for the spectral shape is derived here for low laser intensities in the case of absence of background birefringence and perfectly crossed polarizers. Treating the PS signal in terms of a Degenerate Four-Wave Mixing (DFWM) process [14], we use results derived in [15] for the DFWM spectrum. Cross-correlation effects due to finite laser bandwidth in experimental spectra can then be described by convolution procedures, as carried out by Teets [16] for the case of coherent Anti-Stokes Raman-Spectroscopy (CARS). Assuming equal collisional relaxation rates γ for all rotational components, we then obtain in the first non-vanishing order of perturbation theory for the signal intensity (no saturation):

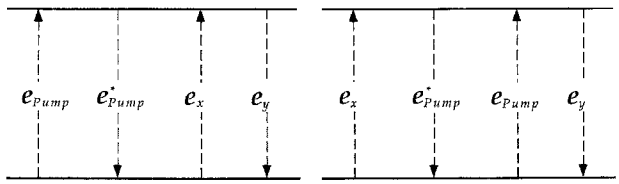

Fig. 1. Polarization spectroscopy in terms of the DFWM process. *Arrows* denote transitions between energy levels of the molecule induced by the interaction with pump ($\mathbf{e}_{\text{pump}}$), probe ($\mathbf{e}_x$) and signal photons ($\mathbf{e}_y$). In the case of co-propagating waves, both scattering channels differing by a permutation of $\mathbf{e}_{\text{pump}}$ and $\mathbf{e}_x$ must be taken into account [17]

$$
\begin{aligned}
I^{\text{PS}} \propto & \int_{-\infty}^{\infty} d\omega \iiint_{-\infty}^{\infty} \Bigg| \sum_{J',a',J,a} P(J',a';J,a) \exp(-E_{J,a}/k_{\text{B}}T) \\
& \times \int_{-\infty}^{\infty} \left(\frac{1}{\mathrm{i}(\tilde{\omega}_1 - \omega_0 + kv) + \gamma} + \frac{1}{\mathrm{i}(\omega_1 - \tilde{\omega}_1 - kv) + \gamma} \right) \\
& \times \frac{\exp(-mv^2/2k_{\text{B}}T)dv}{[\mathrm{i}(\tilde{\omega}_1 - \omega_0) + \gamma][\mathrm{i}(\tilde{\omega}_1 - \omega \pm kv) + \gamma]} \Bigg|^2 \\
& \times I_{\text{L}}(\omega_0) I_{\text{L}}(\omega_1) I_{\text{L}}(\omega_2) \\
& \times \delta(\omega - \omega_2 + \omega_1 - \omega_0) d\omega_0 d\omega_1 d\omega_2, \qquad (1)
\end{aligned}
$$

where $\tilde{\omega}_l$ is the frequency of the molecular transition: $\tilde{\omega}_l = (E_{J',a'} - E_{J,a})/\hbar$, and $I_{\text{L}}(\omega)$ describes the spectral profile of the laser radiation. Within this equation, v denotes the velocity, J the total angular momentum, and a labels the electronic and vibrational state. The absolute value of the wave vector is designated by k, whereas $\pm k$ in the denominator is related to co- and counter-propagating geometry, respectively.

In the case of co-propagating pump and probe beams, the rotational linestrength factor $P(J',a';J,a)$ is determined by two scattering diagrams (Fig. 1) differing by the permutation of pump ($\mathbf{e}_{\text{pump}}$) and probe ($\mathbf{e}_x$) photons [5]:

$$
\begin{aligned}
& P(J',a';J,a) \\
& = \sum_{\substack{m,m',\\ m'',m'''}} (\langle J,m,a|\mathbf{e}_y|J',m',a'\rangle \langle J',m',a'|\mathbf{e}_x|J,m'',a\rangle \\
& \quad \times \langle J,m'',a|\mathbf{e}^*_{\text{pump}}|J',m''',a'\rangle \langle J',m''',a'|\mathbf{e}_{\text{pump}}|J,m,a\rangle \\
& \quad + \langle J,m,a|\mathbf{e}_y|J',m',a'\rangle \langle J',m',a'|\mathbf{e}_{\text{pump}}|J,m'',a\rangle \\
& \quad \times \langle J,m'',a|\mathbf{e}^*_{\text{pump}}|J',m''',a'\rangle \langle J',m''',a'|\mathbf{e}_x|J,m,a\rangle). \qquad (2)
\end{aligned}
$$

The sum over magnetic quantum numbers can be calculated using the approach developed in [17]. For a linearly and circularly polarized pump beam, we have, respectively:

$$
\begin{aligned}
P^{\text{Lin}}(J',a';J,a) = & -\mathrm{i} \left(\frac{2J+1}{2J'+1} \right)^2 C(J',a';J,a) \\
& \times \sum_m (C^{J',m+1}_{J,m;1,1})^2 \, (C^{J',m+1}_{J,m+2;1,-1})^2, \\
P^{\text{Circ}}(J',a';J,a) = & \left(\frac{2J+1}{2J'+1} \right)^2 C(J',a';J,a)
\end{aligned}
$$

$$\times \sum_m (C^{J',m+1}_{J,m;1,1})^2 \,[(C^{J',m+1}_{J,m;1,1})^2 - (C^{J',m-1}_{J,m;1,-1})^2]. \quad (3)$$

Here, $C^{J',m'}_{J,m;1,q}$ denotes a Clebsch-Gordon coefficient [18]. The factors $C(J',a';J,a)$ are independent of the polarization arrangements and can be expressed via reduced matrix elements of the dipole-moment operator μ [17]. From (3), the results for R-, Q- and P-branch transitions ($J' = J-1, J, J+1$, respectively) for a linearly polarized pump beam read:

$$P^{\mathrm{Lin}}(J+1,a';J,a) = \frac{-\mathrm{i}}{15}\frac{2J+1}{(J+1)(2J+3)} \times (2J^2+4J+5)\,C(J',a';J,a)^2, \quad (4a)$$

$$P^{\mathrm{Lin}}(J,a';J,a) = \frac{-\mathrm{i}}{15}\frac{2J+1}{J(J+1)} \times (2J-1)(2J+3)\,C(J',a';J,a)^2, \quad (4b)$$

$$P^{\mathrm{Lin}}(J-1,a';J,a) = \frac{-\mathrm{i}}{15}\frac{2J+1}{J(2J-1)} \times (2J^2+3)\,C(J',a';J,a)^2, \quad (4c)$$

and for a circularly polarized pump beam:

$$P^{\mathrm{Circ}}(J+1,a';J,a) = \frac{1}{3}\frac{2J+1}{(J+1)(2J+3)} \times (2J^2+4J+1)\,C(J',a';J,a)^2, \quad (4d)$$

$$P^{\mathrm{Circ}}(J,a';J,a) = \frac{1}{3}\frac{2J+1}{J(J+1)}\,C(J',a';J,a)^2, \quad (4e)$$

$$P^{\mathrm{Circ}}(J-1,a';J,a) = \frac{1}{3}\frac{2J+1}{J(2J-1)} \times (2J^2-1)\,C(J',a';J,a)^2. \quad (4f)$$

Within the Born-Oppenheimer approximation, the coefficient $C(J',a';J,a)$ is represented by the product of the Frank-Condon factor $|\langle v|v'\rangle|^2$ for the vibrational band under study, the square of the electronic transition matrix element $\langle \Lambda|\mu_q|\Lambda'\rangle$ and the so-called coupling-case factor depending on the rotational quantum numbers. For Hund's coupling case (a), we can write [17]:

$$C(J',a';J,a) = \alpha (C^{J',\Omega'}_{J,\Omega;1,\Omega'-\Omega})^2, \quad (5a)$$

where $\alpha = |\langle v|v'\rangle,^2 |\langle \Lambda|\mu_q|\Lambda'\rangle|^2$.
Similarly [17], for Hund's case (b), one has:

$$C(J',a';J,a) = \alpha(2N+1)(2J+1) \times (C^{N',\Lambda'}_{N,\Lambda;1,\Lambda'-\Lambda})^2 \begin{Bmatrix} N\,S\,J \\ J'\,1\,N' \end{Bmatrix}^2. \quad (5b)$$

Here the expression in the curly brackets denotes $6J$-symbols [18].

Equation (1) was used to numerically analyse spectra for OH and NH radicals. The calculation of the five-dimensional integral can be simplified in the case of non-overlapping spectral lines. Assuming a Lorentzian line shape for a single rotational component, we obtain for the co-propagating beam arrangement:

$$\begin{aligned} I^{\mathrm{PS}}_{\mathrm{Co-p}} \approx & \int_{-\infty}^{\infty} d\omega \iiint_{-\infty}^{\infty} \Bigg| \sum_{J',a',J,a} P(J',a';J,a)\exp(-E_{J,a}/k_{\mathrm{B}}T) \\ & \times \left(\frac{1}{\mathrm{i}(\tilde{\omega}_1-\omega_0)+\tilde{\gamma}} + \frac{1}{\mathrm{i}(\omega_1-\tilde{\omega}_1)+\tilde{\gamma}}\right) \\ & \times \frac{1}{[\mathrm{i}(\omega_1-\omega_0)+\gamma][\mathrm{i}(\tilde{\omega}_1-\omega)+\tilde{\gamma}]}\Bigg|^2 \\ & \times I_{\mathrm{L}}(\omega_0)\,I_{\mathrm{L}}(\omega_1)\,I_{\mathrm{L}}(\omega_2)\,\delta(\omega-\omega_2+\omega_1-\omega_0) \\ & \times d\omega_0\,d\omega_1\,d\omega_2 \\ \approx & \frac{4\pi\tilde{\gamma}^2}{\gamma} \iint_{-\infty}^{\infty} I_{\mathrm{L}}(\omega_0)^2\,I_{\mathrm{L}}(\omega)\,d\omega\,d\omega_0 \\ & \times \Bigg| \sum_{J',a',J,a} P(J',a';J,a)\exp(-E_{J,a}/k_{\mathrm{B}}T) \\ & \times \frac{1}{[(\tilde{\omega}_1-\omega_0)^2+\tilde{\gamma}^2][\mathrm{i}(\tilde{\omega}_1-\omega_l)+\tilde{\gamma}]}\Bigg|^2. \end{aligned} \quad (6)$$

Here, $\tilde{\gamma}$ is an "effective" linewidth including both collisional and Doppler broadening. The second equality in (6) is valid if the relaxation rate γ is much less than the total linewidth $\tilde{\gamma}$. Treating $\tilde{\gamma}$ as a "fitting parameter" this relatively simple expression can be applied to spectral fitting. In fact, spectral contours described by (6) and (1) are slightly different only in the line wings.

2 Experimental setup

For the co-propagating beam geometry, the experimental setup is shown in Fig. 2. A frequency-doubled dye laser (Spectra Physics, PDL-1A) pumped by a Nd:YAG laser (Spectra Physics, GCR3, pulse duration 5–7 ns) generated tunable radiation in the spectral region around 335 and 308 nm, using DCM or sulforhodamin 101 in methanol, respectively. The linewidth of the UV output was approximately 0.4 cm^{-1} (FWHM). Inserting an intracavity etalon into the oscillator of the dye laser, its linewidth could be reduced down to 0.08 cm^{-1}. The laser radiation was split into two beams by a quartz plate (9 mm thick) to form a strong pump and a weak probe beam. The pump beam passed a half-wave plate before it entered a polarizer (Halle, extinction ratio better than 10^{-5}) forming a variable beam attenuator. Circularly polarized light was generated by inserting an additional quarter-wave plate behind the polarizer. The probe beam passed a pair of crossed polarizers (extinction ratio better than 10^{-5}) before it reached a spatial filter for straylight suppression. The signal was detected by means of a Photo Multiplier Tube (PMT) (Hamamatsu, 1P28). In front of the PMT, an interference filter (centre wavelength: 337 nm, FWHM: 10 nm; centre wavelength: 300 nm, FWHM: 70 nm) minimized background radiation. A small fraction of the pump beam was split off to monitor the laser energy. The depicted co-propagating beam geometry was used for the investigation of the saturation behavior of the polarization signal as a function of pump-beam intensity, whereas the

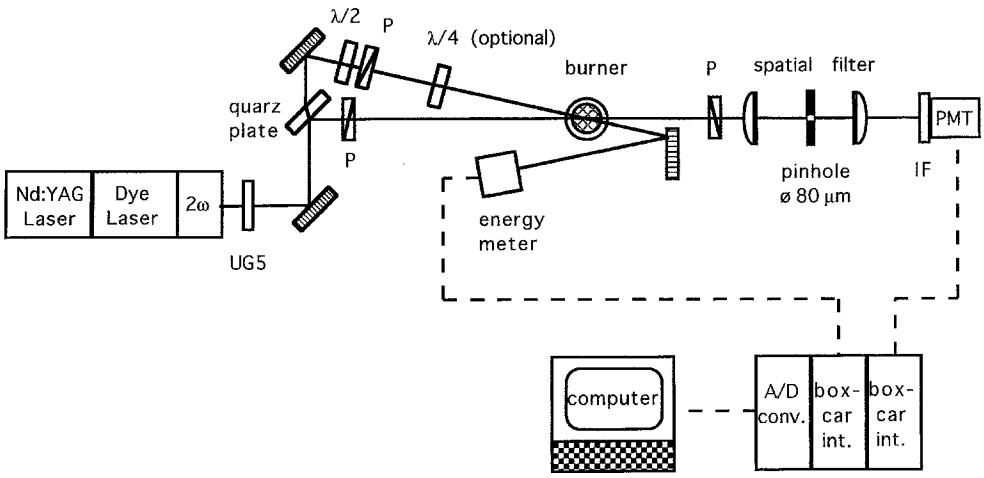

Fig. 2. Experimental set-up of polarization spectroscopy with co-propagating beam geometry. (P: polarizer, PMT: photomultiplier tube, IF: interference filter, 2ω: frequency-doubling (KDP) crystal)

counter-propagating beam geometry was used to investigate the accompanying line broadening with Doppler-free spectral resolution.

The electrical signals were captured with gated integrators (SRS) and fed to a pen recorder (Philips) and a laboratory computer (Hewlett Packard). The OH and NH radicals were generated in atmospheric pressure flames operated with premixed fuel/oxidizers, methane/air, and ammonia/oxygen, respectively. The beams crossed approximately 8 mm above the burner head with an angle of $\approx 4°$.

3 Results

Spectra of the R and Q branches of the $A^2\Sigma^+ - X^2\Pi$ and the $A^3\Pi - X^3\Sigma$ (0–0) electronic bands of OH and NH were investigated, respectively. Saturation effects on signal intensity and lineshape were studied for selected transitions. For all R-branch measurements, a circularly polarized pump beam, and for Q-branch measurements, a linearly polarized pump beam with its direction of polarization rotated 45° relative to the probe-beam polarization, was used.

3.1 OH-measurements

Figure 3a depicts the R_1 and R_2 band heads of OH in the methane/air flame. In this case, a co-propagating beam geometry was used. Each data point was averaged over 10 laser shots. Pulse energies of pump and probe beam were typically 100 and 4 µJ, respectively, within a beam cross section of 10 mm^2 (calculated from the beam diameter as measured by the translation of a 100 µm diameter pinhole in front of the detector). Under similar conditions, parts of the Q_1 and Q_2 branches were recorded (Fig. 3b). The signal-to-noise ratio on the strongest lines was found to be better than 1000:1. In order to investigate the power dependence of the signal intensity, the laser was tuned to the line centre of the $R_1 9$ transition, and the pump-beam intensity was varied from 0.02 to 1.8 MW/cm^2 by rotating the half-wave plate in front of the polarizer in the pump-beam path. The intensity of the probe beam was kept constant at 0.018 MW/cm^2. For the case of a counter-propagating beam geometry, the result is depicted in Fig. 4a. According to (1), for non-saturating conditions, the polarizers perfectly crossed and no background biref-

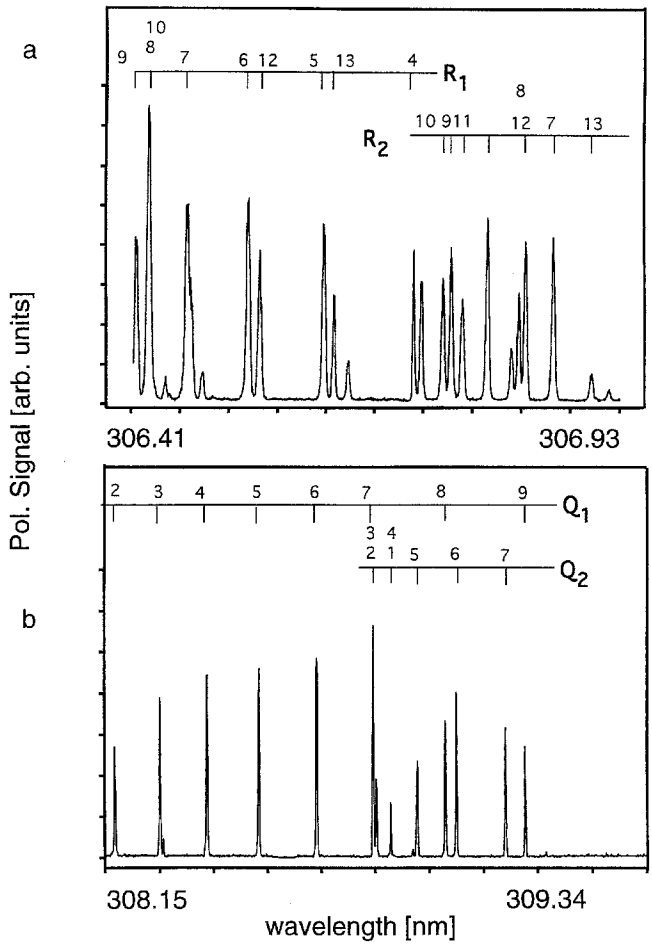

Fig. 3a, b. Polarization spectra of the R (**a**) and Q branch (**b**) of OH ($A^2\Sigma - X^2\Pi$) recorded in an atmospheric pressure methane/air flame. Co-propagating pump and probe beam

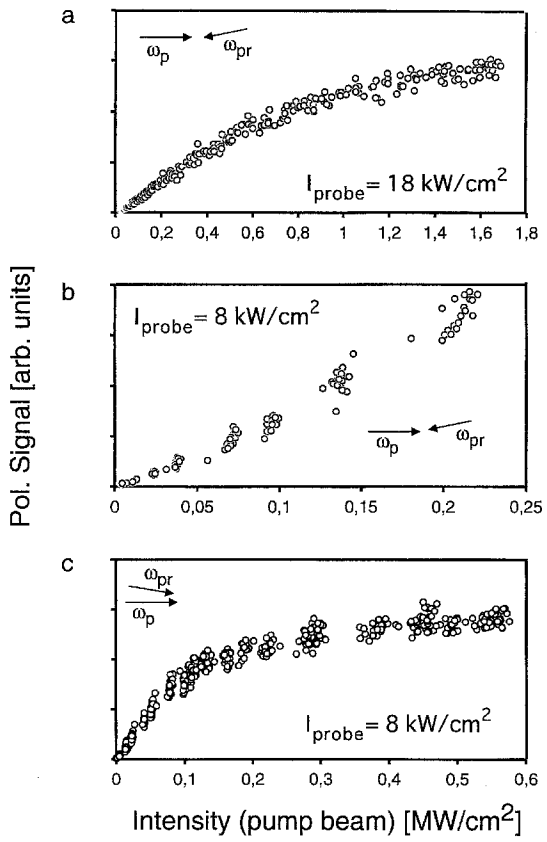

Fig. 4a–c. Pump-beam intensity dependence of the polarization-spectroscopy signal for OH (**a**) and NH (**b**) in the counter-propagating and for NH (**c**) in the co-propagating beam geometry. For OH the $R_1 9$ and for NH the $R_3 5$ line was used

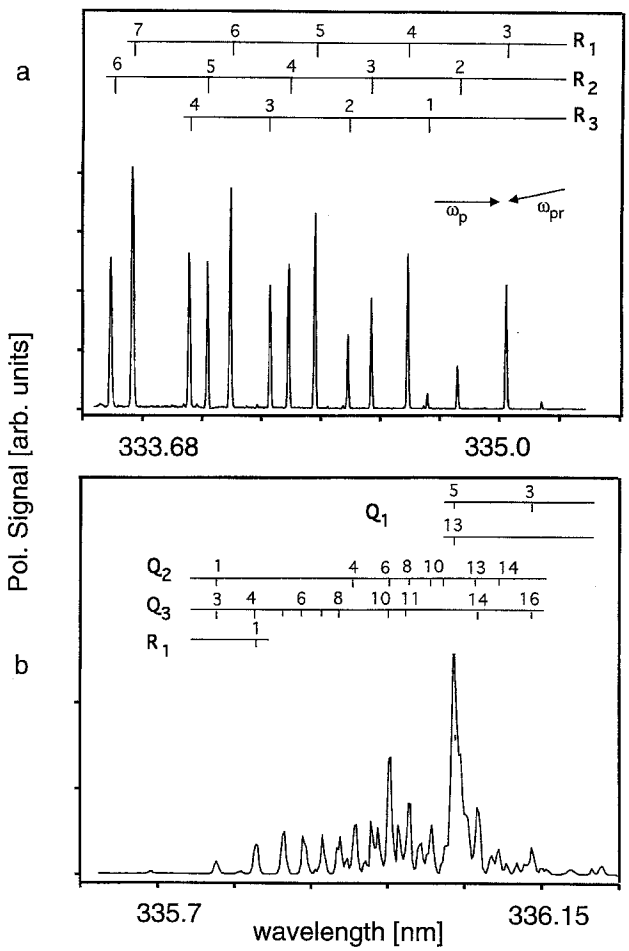

Fig. 5a, b. Polarization spectroscopy spectra of parts of the R (**a**) and Q branch (**b**) of NH recorded in an atmospheric pressure ammonia/oxygen flame. Counter-propagating pump and probe beam

ringence the signal intensity should vary with the pump-beam intensity squared. It is clearly seen in the figure that saturation starts to set in from pump-beam intensities as low as 0.1 MW/cm^2. Above this value the signal intensity rises linearly with pump-beam intensity and finally approaches a constant value. The accompanying line broadening was investigated with the line-narrowed output of the dye laser (intracavity etalon, FWHM 0.08/cm) and a counter-propagating beam geometry to eliminate Doppler broadening. For a constant probe-beam intensity of 0.018 MW/cm^2 but different pump-beam intensities, the frequency was scanned across the $R_1 9$ absorption line by pressure tuning the oscillator. Despite a significant fraction of the instrumental contribution to the measured overall linewidth, saturation increases the linewidth for pump-beam intensities larger than 0.4 MW/cm^2, reaching 0.12 cm^{-1} (FWHM) at 1.1 MW/cm^2.

3.2 NH measurements

Close to the flame front in the ammonia/oxygen flame, NH could unambiguously be identified by its prominent spectral structure. In Figs. 5a and b, spectra of R and Q branches are shown using the counter-propagating beam geometry. Data acquisition and beam intensities were chosen similar to the OH measurements. The signal-to-noise ratio for the strongest transitions was found to be better than 1000:1. While the probe-beam intensity was kept constant at 0.008 MW/cm^2, the saturation behavior was investigated for the $R_3 5$ line by varying the pump-beam intensity from 0.008 to 0.24 MW/cm^2 for the counter-propagating (Fig. 4b) and from 0.008 to 0.6 MW/cm^2 for the co-propagating beam geometry (Fig. 4c). As can be seen, the onset of saturation is shifted to lower pump-beam intensities for co-propagating than for counter-propagating beams due to better matching between laser bandwidth and Doppler-broadened NH absorption lineshape. On the other hand, for the counter-propagating-beam arrangement, the signal intensity does not show any tendency to level off within the pump-beam intensity range investigated here (Fig. 4b). Again, the specific line broadening due to saturation of the $R_3 5$ line was carried out similarly to the OH measurements using the etalon-narrowed dye laser. Saturation broadening was observed to be significant above a pump-beam intensity of 0.2 MW/cm^2.

4 Spectral simulation

For OH and NH, Figs. 4a–c show that saturation is noticeable for pump-beam intensities lower than 0.1 MW/cm^2. Therefore, care has to be taken if temperatures from experimental data are evaluated using a theoretical approach where saturation is not taken into account. In this work, spectral fitting has been done for polarization spectra of OH recorded with very low beam intensities of 50 kW/cm^2 for the pump and 8 kW/cm^2 for the probe, respectively. For this investigation, a co-propagating beam geometry was used. These experimental conditions still gave a sufficient signal-to-noise ratio of about 40:1. Using the theoretical approach presented above, a synthetic spectrum was fitted to the R_1 band head assuming Hund's coupling case (a). Term values for calculating transition frequencies were taken from [19]. The result is shown in Fig. 6a. The residuum between measurement and simulation is plotted at the bottom of the figure. The laser's spectral bandwidth was fixed to 0.6 cm^{-1} (FWHM). The best fit resulted in a temperature of 2120 K and a collision-broadened bandwidth of 0.2 cm^{-1} (FWHM). When Hund's case (b) was employed in the line-strength calculation – an assumption which for OH is justified for high rotational quantum numbers – a fit of comparable quality was obtained giving a temperature 100 K higher than for Hund's case (a). In our situation, where rotational levels between 7 and 11 are probed, the coupling of rotational and electronic angular momentum is considered to lie in between Hund's cases (a) and (b). Unfortunately, the temperature profile of the burner used in this study was not characterized by independent methods, which left the true temperature in the measurement point unknown. However, from CARS and DFWM measurements with the same type of burner using propane as fuel [20], temperatures at the probe volume should be less than 2140 K. It is obvious from these results that, for accurate temperature derivations from polarization spectra, not only qualitatively good spectral fits, but also proper line-strength calculations are necessary.

We recorded spectra in the same wavelength range as given in Fig. 6a using somewhat higher pump-beam intensities (360–1080 kW/cm^2). Spectral fits to these data looked very similar to that in Fig. 6a, but resulted in much higher temperatures. For pump-beam intensities of 360, 820, 1080 kW/cm^2, temperatures of 2391, 2690, 3549 K, respectively, were obtained. This examination reveals the sensitivity of spectral modeling in polarization spectroscopy to saturation effects. For the future, a theoretical approach has to be developed, where saturation is taken into account, since useful signal-to-noise ratios in practical measurements mostly involve higher laser intensities. In addition, it can be expected, similar to investigations in DFWM [21], that signals in polarization spectroscopy are less affected by collisions under saturating conditions.

For a more detailed theoretical description of the spectral shape, one has to consider the influence of saturation and the relaxation of molecular orientation or alignment. The relaxation rates of molecular orientation and alignment for OH have been investigated recently for the same burner and electronic state used in this study [22].

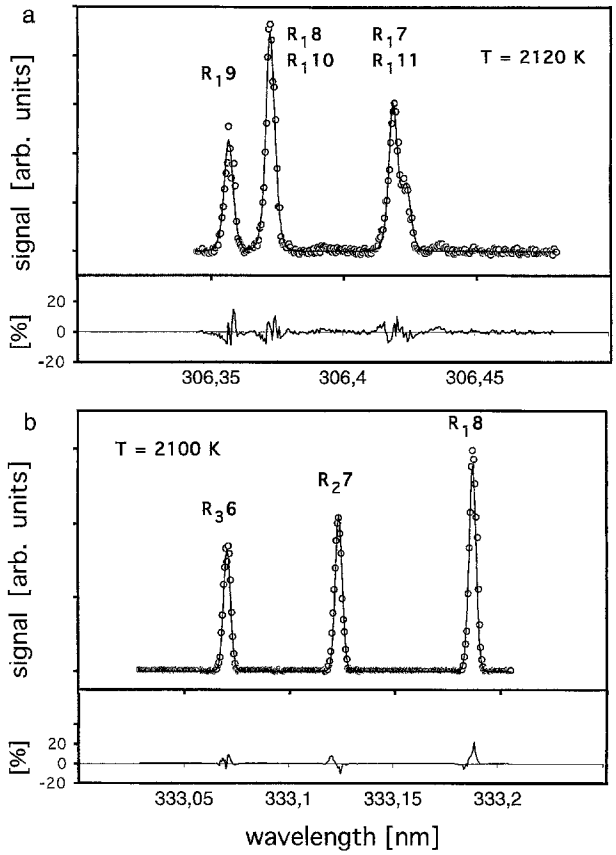

Fig. 6a,b. Comparison between experimental (*circles*) and calculated (*solid line*) polarization spectra of OH and NH. For OH (**a**) Hund's case (a) and (6) (in this equation it is assumed that the relaxation rate γ is much less than the total linewidth $\tilde{\gamma}$) was used for a temperature fit. For NH (**b**) Hund's case (**b**) and (4d) was employed

For NH a theoretical spectrum was calculated for a small section of the R branch including the temperature-insensitive $R_1 8$, $R_2 7$, $R_3 6$ triplet using (1) (nomenclature and term values are given in [23]) for an assumed temperature of 2100 K and a bandwidth of 0.2 cm^{-1} (FWHM) originating from collisional broadening. The bandwidth of the laser was measured to 0.4 cm^{-1} (FWHM) for this spectral region. It has to be noted that using the accurate expression from (1) no fit procedure was used. The results obtained using $(+k)$ in the denominator of (1) is compared to experimental data recorded in the co-propagating beam geometry. The purpose was to see if the correct lineshape for these transitions was calculated.

This triplet shows no temperature sensitivity because the probed transitions originate from the same rotational level in the electronic ground state, but show different spin components ($S = 0, \pm 1$). In addition, the lines are well isolated which circumvents problems of interference effects and also makes them good candidates for the study of laser-bandwidth convolution procedures in modeling of nonlinear spectra. The result of this comparison is shown in Fig. 6b, where Hund's case (b) was assumed. Relative line intensities and shapes are reproduced quite well for this coupling case. When Hund's coupling case (a) was assumed, the result of calculating relative line intensities

for these transitions was unacceptable in comparison with experiment.

5 Conclusions

In this study, we focused on saturation effects and spectral modeling in polarization spectroscopy for practical applications. For the OH ($A^2\Sigma$–$X^2\Pi$) and NH ($A^3\Pi$–$X^3\Sigma$) (0–0) electronic transitions, saturation is manifested in the leveling-off of the signal intensity as well as in noticeable line broadening with increasing pump-beam intensity. These intensity-dependent deviations from predictions given by a linear treatment come into play already for pump-beam intensities as low as 0.1 MW/cm^2 and have to be considered in practical quantitative measurements of, e.g., temperature or concentration. These conclusions are confirmed by spectral modeling of polarization-spectroscopy signals for these two species using a theoretical approach which takes into account cross-correlation effects in nonlinear signal generation due to finite laser bandwidth. Spectra of R- and Q-branch transitions for OH and NH were recorded with various pump-beam intensities. Spectral fits were perfomed for small parts of the R branches (OH: R_1 band head, NH: $R_1 8$, $R_2 7$, $R_3 6$ lines). In the case of OH, only for experimental conditions where saturation could be excluded, an adequate temperature was obtained. For OH, Hund's case (a) gave the best results. Using Hund's case (b) for OH, the fit temperature was $\approx$ 100–150 K higher. For NH, only Hund's case (b) was successful in reproducing the measured line intensities and shapes assuming a temperature of 2100 K and a pressure-broadened bandwidth of 0.2 cm^{-1}. Because a good signal-to-noise ratio (better than 100:1) is obtained only for saturating conditions, a theoretical approach has to include saturation effects. This will make polarization spectroscopy an attractive method for thermometry, suitable for free-burning flames or for experimental conditions where background birefringence from optical elements in the beam path can be suppressed. At a later stage besides contributions from saturation to line broadening, relaxation of molecular orientation and alignment may be included in the theoretical description of the spectral structure.

Acknowledgements. A.D., T.D. and A.A.S. are grateful to the Deutsche Forschungsgemeinschaft for financial support (grant Dr 195/5 and SFB 359).

References

1. C. Wieman, T.W. Hänsch: Phys. Rev. Lett. **36**, 1170 (1976)
2. K. Danzmann, K. Grützmacher, B. Wende: Phys. Rev. Lett. **57**, 2151 (1986)
3. N.W. Carlson, A.J. Taylor, A.L. Schawlow: Phys. Rev. Lett. **37**, 683 (1976)
4. R.E. Teets, F.W. Kowalski, W.T. Hill, N. Charlson, T.W. Hänsch: Proc. Soc. Phot. Opt. Instr. Eng. **113**, 80 (1977)
5. M. Sargent III: Phys. Rev. A **14**, 524 (1976)
6. W. Demtröder: *Laser Spectroscopy*, Springer Ser. Chem. Phys., Vol. 5 (Springer, Heidelberg, Berlin, 1988)
7. G. Kychakoff, R.D. Howe, R.K. Hanson: Appl. Opt. **23**, 1303 (1984)
8. W.G. Tong, E.S. Yeung: Anal. Chem. **57**, 70 (1985)
9. G. Zizak, J. Lanauze, J.D. Winefordner: Appl. Opt. **25**, 3242 (1986)
10. K. Nyholm, R. Maier, C.G. Aminoff, M. Kaivola: Appl. Opt. **32**, 919 (1993)
11. K. Nyholm, R. Fritzon, M. Aldén: Opt. Lett. **18**, 1672 (1993)
12. K. Nyholm, R. Fritzon, M. Aldén: Appl. Phys. B **59**, 37 (1994)
13. K. Nyholm: Opt. Commun. **111**, 66 (1994)
14. A.A. Suvernev, N.L. Suverneva: Phys. Rev. A **51** (1995) (in press)
15. E.J. Friedman-Hill, L.A. Rahn, R.L. Farrow: J. Chem. Phys. **100**, 4065 (1994)
16. R.E. Teets: Opt. Lett. **9**, 226 (1984)
17. H. Bervas, S. Le Boiteux, L. Labrunie, B. Attal-Trétout: Mol. Phys. **79**, 911 (1993)
18. D.A. Varshalovich, A.N. Moskalev, V.K. Khersonskii: *Quantum Theory of Angular Momentum*, (World Scientific, Singapore 1988) p. 271
19. J.A. Coxon: Cdn. J. Phys. **58**, 933 (1980)
20. T. Dreier, D. Rakestraw: Appl. Phys. B **50**, 479 (1990)
21. R.P. Lucht, R.L. Farrow, D.J. Rakestraw: J. Opt. Soc. Am. B **10**, 1508 (1993)
22. A. Dreizler, R. Tadday, A.A. Suvernev, M. Himmelhaus, T. Dreier, P. Foggi: Chem. Phys. Lett. (1995) (in press)
23. C.R. Brazier, R.S. Ram , P.F. Bernath: J. Mol. Spectrosc. **120**, 381 (1986)